

# Improved Extraction of Objects from Urine Microscopy Images with Unsupervised Thresholding and Supervised U-net Techniques

Abdul Aziz, Harshit Pande, Bharath Cheluvvaraju, Tathagato Rai Dastidar

SigTuple Technologies Pvt. Ltd, Bengaluru, India

abdul,harshit,bharath,trd@sigtuple.com

## Abstract

*We propose a novel unsupervised method for extracting objects from urine microscopy images and also applied U-net for extracting these objects. We fused these proposed methods with a known edge thresholding technique from an existing work on segmentation of urine microscopic images. Comparison between our proposed methods and the existing work showed that for certain object types the proposed unsupervised method with or without edge thresholding outperforms the other methods, while in other cases the U-net method with or without edge thresholding outperforms the other methods. Overall the proposed unsupervised method along with edge thresholding worked the best by extracting maximum number of objects and minimum number of artifacts. On a test dataset, the artifact to object ratio for the proposed unsupervised method was 0.71, which is significantly better than that of 1.26 for the existing work. The proposed unsupervised method along with edge thresholding extracted 3208 objects as compared to 1608 by the existing work. To the best of our knowledge this is the first application of Deep Learning for extraction of clinically significant objects in urine microscopy images.*

## 1. Introduction

Microscopic examination of urine samples is often prescribed by a clinician for diagnosing various diseases. Such microscopic examination is used to detect and identify clinically important objects in urine. These objects are usually Red Blood Cells (RBCs), White Blood Cells (WBCs), epithelial cells, casts, bacteria, yeast, parasites, mucus, sperms, crystals, and artifacts [23]. Apart from the objects of clinical importance, a urine sample may contain large amounts of artifacts and indeterminate objects. These entities can be present due to multiple reasons, ranging from a thread being present in the urine sample to out-of-focus objects and lens artifacts. We collectively call such unimpor-

tant entities artifacts. A qualified medical practitioner observes multiple fields of view (FOVs) of a urine sample under the microscope. For each FOV, the medical practitioner identifies and quantifies these objects by manually focusing and zooming in on different regions in the FOV. Fig. 1 shows an example of an FOV image. Examples of various objects and artifacts found in an FOV image are shown in Fig. 2.

Manual microscopy, though time consuming, is considered the gold standard in microscopic urine examinations. However different pathologists often generate inconsistent reports. Hence there is a need for an efficient and accurate automated urine analyzer that helps in disease diagnostics, by boosting the productivity of pathologists, bringing in consistency in test results, and shortening the turn around time for reporting. To build a highly accurate automated analyzer, the first step is to extract image patches of urine objects from a microscopic image of urine samples. Extraction of urine objects is critical for an automated urine analyzer as classification and other quantification steps are dependent on extraction of objects. For an FOV image, a perfect extraction algorithm should be able to extract all the objects present in the FOV image and ignore all the artifacts present in the FOV image. If the output of an extraction module is input to a classification module, then sending too many artifacts to the classifier may cause generation of too many false positives for different objects by misclassification of the artifacts as resembling object types. One can add artifact as another class in the subsequent classifier, and it helps to some extent. But a classifier may not be able to learn all the features of the artifact class because of its undefined nature. When we discuss extraction of objects from urine images, not only do we need segmentation of cells and other objects from the background, but we also need to minimize the number of artifacts that get extracted along with the objects. In this paper we propose methods that show improvement in extraction of objects from urine microscopy images over existing methods. In this section, we first discuss certain challenges in extraction of urine ob-

jects, and then discuss the key contributions of this paper.



Figure 1. A microscopic field of view (FOV) of a urine sample.

### 1.1. Challenges in extraction of urine objects

Following challenges are associated with extraction of objects in urine microscopy images:

- **Variability in quality of capture:** The images captured for an FOV vary greatly based on the capture mechanism for the sample. Slight change of focus of camera may result in remarkable differences in appearance of objects. An example is shown in Fig. 3. Simple rules based on sharpness and size may not be very effective in this scenario.
- **Variability in the size and shape of objects:** As seen in the Fig 2, both objects and artifacts vary greatly in size and shape. Hence, rules based on shape and size

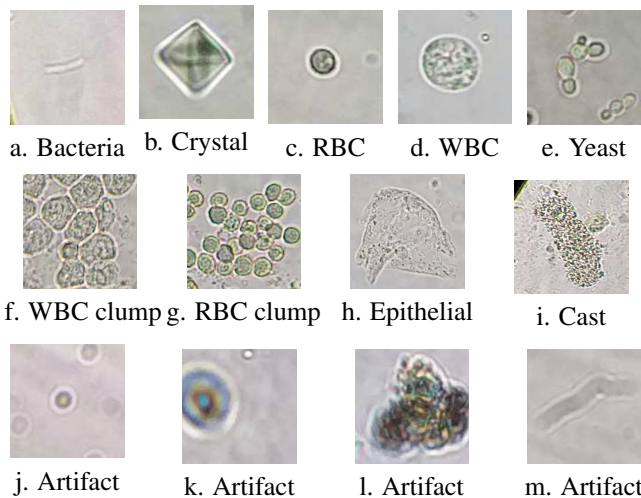
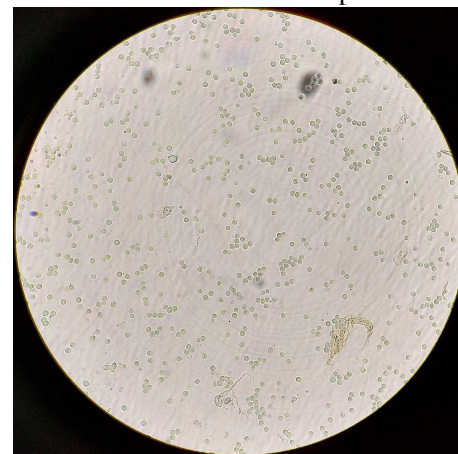


Figure 2. Examples of objects of clinical importance (a-i) and artifacts (j-m). Note: cast and epithelial are significantly scaled down.



a. Out-of-focus FOV capture



b. Optimally focused FOV capture

Figure 3. FOVs captured at slightly different focal depths.

for distinguishing objects from any other artifacts or impurities are not effective for extraction.

- **Partial focus due to multilayer sample:** Urine samples in slides form multilayer fluid with depth of approximately 20 microns. Objects can be suspended at different depths in the fluid depending on their specific gravity and thus have different optimal focal depths. Capturing a single image in one FOV may not include all the relevant objects in their optimally focused state. Some objects may be blurred.
- **Presence of artifacts:** Artifacts are clinically insignificant and can be introduced in a sample as alien objects or lens artifacts during capture of FOVs. Close resemblance of certain impurities to objects can cause an extraction mechanism to extract them as false positives. Fig. 2 (j) and (m) show artifacts introduced by capture device and Fig. 2 (k) and (l) show artifacts caused by alien objects. The round artifacts in Fig. 2 (j) and (k) are similar in shape to RBC and WBC (Fig. 2 (c) and

(d) respectively and thus an extraction algorithm may end up extracting many such artifacts when trying to extract RBCs and WBCs.

- **Low contrast images:** As can be seen from Fig. 2, certain objects such as bacteria and epithelial cells in urine have low contrast when compared to background, which makes it further challenging to extract these objects without adding false positives from the background.

## 1.2. Contributions

The key contributions of this paper are as follows:

- We propose an unsupervised method for extraction of objects in urine FOV images. This method is based on Sauvola's adaptive binarization method [20].
- We also apply U-net [19] for extraction of objects from urine FOV images. To the best of our knowledge this is the first application of Deep Learning architectures such as U-net for urine object extraction.
- We merge the second thresholding technique proposed by Liancheng *et al.* [11] (which we call edge thresholding), which separates adhesive cells by removing edges, with our proposed techniques and compare the performance of the proposed unsupervised method, U-net method, unsupervised with edge thresholding, U-net with edge thresholding, and the method by Liancheng *et al.* [11]. We show that our proposed methods significantly outperform the existing method.

This paper is organized as follows: Section 2 discusses the existing work in extraction of objects in urine microscopic images along with the discussion on Deep Learning architectures that can be used for extraction of objects. Section 3 discusses the proposed methods for extracting urine objects from FOV images. Section 4 describes the data sets used in training and testing in this study. Section 5 presents the results and the performance comparison between our proposed methods and the existing method by Liancheng *et al.* [11]. In this section we also discuss further analysis of extraction results for all the methods and all the types of objects. Finally, Section 6 concludes the paper.

## 2. Related Work

Image processing and computer vision techniques have earlier been applied to extraction of various objects in a urine samples. Early attempts limited to segmenting blood cells in urine images are by Luo *et al.* [13] using Mumford-Shah model [14] and by Jiang *et al.* [7], in which they used a combination of the level set method [16] and a simplified Mumford-Shah model [2]. A method using wavelet

transform along with edge detection and adaptive thresholding [10] was used to segment WBCs, RBCs, epithelial cells, and casts. Cellular neural networks [28] were deployed to segment WBCs and epithelial cells. Gabor filters along with simulated annealing and K-means clustering [27] were also used for segmenting urinary images, but this was shown to work only for small patches of size 128x128 pixels, while microscopic urine images are much larger in size. For segmenting only casts, an adaptive bi-threshold segmentation using histogram of the variance mapping image [9] was proposed. A combination of coarse segmentation using contourlet transform followed by a finer segmentation using a level set method was also explored [3]. For segmenting only RBCs multiple methods such as a Sobel operator variant along with Hough transform [1], Sobel edge enhancement along with Otsu's binarization [29], and watershed algorithm [4] were used. For segmenting bigger objects such as cast and epithelial cells, Wu and Kang [26] used a simple combination of Sobel edge detection with edge enhancement algorithm. A strategy that combines adaptive thresholding, distance transform and watershed algorithm was deployed to address the segmentation of adhesive cells such as RBC clumps and WBC clumps [21]. Recently, Liancheng *et al.* [11] proposed a segmentation method based on standard deviation gradient with dual-threshold, where the first threshold gives the over all segmentation while the second threshold is combined with the first threshold to segment adhesive cells.

A method that minimizes the extraction of artifacts, which tends to get confused with object classes in the downstream classification methods, hasn't been studied in existing works on urine object extraction. Most of the extraction studies lack a comparison with previous extraction methods, which we will address in this paper by comparing our proposed method with the recently proposed method by Liancheng *et al.* [11].

The state-of-the-art results yielded by the recent Deep Learning techniques started with CNN variants for classification tasks by architectures such as AlexNet [8], VGGNet [22], GoogLeNet [25], ResNet [5], and DenseNet [6]. These opened avenues for Deep Learning architectures in other tasks as well. With the advancements in architectures such as fully convolutional networks (fCNN) [12] and U-net [19] deep learning gained popularity in biomedical image segmentation as well. By rewriting fully connected layers as convolutions and using the shift-and-stitch techniques, fCNN [12] was successful in segmentation of images using only convolution layers by adapting popular classification networks for segmentation. U-net [19] builds upon fCNN by modifying the architecture by supplementing usual contracting layers with upsampling operators for increasing the image size. Taking inspiration from ResNet [5], U-net also uses skip-connections to di-

rectly connect opposing contracting and expanding convolutional layers. Thus U-net produced state-of-the-art results in segmentation tasks as well. This motivated us to also apply segmentation using U-net to the urine object extraction problem.

### 3. Proposed Methods

Input for the extraction is a single RGB FOV image ( $4032 \times 3024$  pixels) where 5 pixels correspond to 1 micron. We first describe the proposed unsupervised method.

#### 3.1. Proposed unsupervised extraction

For designing an unsupervised extraction method, we experimented with multiple variants of thresholding methods such as Otsu's method [17], Niblack's method [15], and Sauvola's method [20]. We found that Sauvola's method was the most promising given the blurry objects and noisy background in FOVs caused by artifacts and also in binarization of low contrast images which is the case in urine sample FOV images. So, the proposed unsupervised method uses Sauvola's method as a key component. The following steps are used to extract patches from a single FOV image:

1. Apply a global threshold mask on the FOV image to separate the illuminated circle from the surrounding dark regions (see Fig. 1) and then apply CLAHE [18].
2. Apply the Sauvola's image binarization method [20] to separate foreground objects from background with window size  $w = 15$  and bias  $k = 0.2$
3. Do adaptive dilation on the binary image:
  - (a) dilate with kernel size  $d$  for  $n$  iterations
  - (b) if area of biggest contour [24]  $\geq 10\%$  of FOV area and  $n > 1$  then repeat 3 (a) with  $n \leftarrow n - 1$ , else go to 3(c)
  - (c) if area of biggest contour  $\geq 10\%$  of FOV area and  $d > 1$  then repeat 3(a) with  $d \leftarrow d - 2$ , else go to 4
4. Discard the contours with area  $\leq T_{\text{area}}$
5. Find centroid and bounding box for each contour

In the above algorithm, we started with  $d = 7$  and  $n = 3$ . The area threshold  $T_{\text{area}} = 500$  square pixels (20 square microns).

We now describe how we used U-net as the supervised extraction method.

#### 3.2. Proposed U-net based extraction

U-net input size is a  $64 \times 64$  and 3 channel RGB image. The contracting path has three blocks and each of them consists of two convolutional layers. For the first two blocks,

max-pooling is applied after two successive convolutions in each block. Transpose convolution is applied to increase the size of the input after two convolutions. The next two layers are the same as third layer with concatenation of corresponding output from the contracting path as their input. The exact architecture achieved via cross validation and the corresponding hyper parameters are presented in Fig. 4. The following steps are followed to extract patches from a trained U-net given an FOV image.

1. Crop out the FOV region from the image.
2. Create overlapping patches of size  $64 \times 64$  with stride size 32.
3. Invoke the trained U-net model on the patches. The output has two stacked matrices of probabilities for each pixel being in foreground or background. For overlapping pixels across different patches the average of the probabilities is taken. This generates the probability map for the whole FOV.
4. Apply a global thresholding on the FOV probability map to obtain segmentation mask.
5. Apply morphological opening on the mask and find contours [24] in the mask to get the regions of enclosing objects. Discard contours whose area is less than  $T_{\text{area}}$ .
6. Take patches around the object enclosing the respective contours.

In the above algorithm we used area threshold  $T_{\text{area}} = 500$  square pixels.

Now we describe a key module applicable to the proposed extraction methods called **edge thresholding**, which is not a very useful step in isolation but it helps in extracting adhesive objects when applied as a second step after any of the two proposed methods. This technique is proposed by Liancheng *et al.* [11] as the second thresholding in their dual threshold method. The purpose of this method is to find edges using grayscale distribution of the image and remove those edges to separate adhesive cells from the original segmentation mask.

#### 3.3. Edge Thresholding

Input to the edge thresholding technique is the FOV image and the segmentation mask obtained from either the unsupervised method or the U-net method. The key steps in edge thresholding post first level of segmentation are:

1. Calculate the histogram  $H$  of the grayscale value for FOV image and find  $k$  such that  $H[k] = \max(H[i])$ .
2. Set threshold  $T_{\text{edge}} = k + \beta$  where  $\beta$  is in the range of 10 to 40.

3. Binarize the FOV image using the above threshold  $T_{\text{edge}}$ . This will give the edge mask.
4. Remove the pixels from the original segmentation mask which are present in edge mask.

In this paper  $\beta$  is set to 25.

## 4. Dataset

We have a **test data** of 50 microscopic FOV images of the type shown in Fig. 1. These images were captured from a microscopic device with magnification of 400X for evaluating and comparing the performance of the proposed and the existing extraction methods. Each image corresponds to a single FOV of a urine sample under the microscope. The images were captured from different samples to include different types of urine objects such are bacteria, crystal, cast, epithelial cell, RBC, WBC and yeast. For training the U-net model, an expert pathologist created 4150 binary segmentation masks from 329 FOV images as square image patches of size  $64 \times 64$  pixels. These urine samples contribute to **training data** and are completely independent of the test data. The class-wise distribution of the masks of the **training data** are shown in Table 1. 30% of the training data was used as a validation set for tuning the hyperparameters of the U-net. On a pixel level the foreground pixels consisted of 37% of the total pixel corpus.

## 5. Results and Discussion

Cross validation over various hyperparameters of U-net led to the choice of the architecture and hyperparameters shown in the Fig. 4. The cross validation was done on the validation set described in Section 4.

We computed the segmentation masks using the proposed techniques and the existing technique by Liancheng *et al.* [11] and found connected components with the contours of segmentations. The components were extracted and patches of images were created using bounding box squares around the components. These patches were presented to an expert panel of 3 pathologists, who annotated the patches as either artifacts or one of the other 7 types of urine objects. These annotations served as the ground truth for the labels of the extracted patches. The total count for each type of urine objects and artifacts was recorded and compared. The counts are listed in Table 2. A patch was annotated as an object of a certain type if the proposed mask covers more than 20% of the same object type area. Otherwise it is marked as a false positive i.e. it is put into artifact class. Now we discuss some interesting observations in the results and their analysis.

As seen in Table 2, for both proposed unsupervised extraction and proposed U-net based extraction, more RBCs were extracted with edge thresholding in comparison to

Class	Patch counts
Bacteria	387
Cast	450
Crystal	1039
Epithelial	504
RBC	374
WBC	255
Yeast	234
Artifact	907

Table 1. Class-wise patch distribution for the U-net training dataset.

the corresponding proposed technique without edge thresholding. We would like to reiterate that the method by Liancheng *et al.* [11] already has edge thresholding as it's second module. Edge thresholding can help in segmenting adhesive cells like RBC clumps and WBC clumps in many cases. Some of the examples are shown in Fig. 5 and Fig. 6. In Fig. 5 it can be seen that a clump of RBC was extracted as a single connected component by both the proposed unsupervised extraction method (Fig. 5a) and the proposed U-net method (Fig. 5d). While they were divided into 7, 4 and 5 components in the proposed unsupervised extraction with edge thresholding (Fig. 5b), Liancheng *et al.* [11] (Fig. 5c) and U-net with edge thresholding (Fig. 5e) methods respectively. Similarly the patch of clump of WBC in Fig. 6 was further divided into multiple components by the proposed methods which includes edge thresholding. However, one may notice in Table 2 that while the count of extracted WBCs increases when edge thresholding is applied with the proposed unsupervised extraction but the count of extracted WBCs decreases when edge thresholding is applied with the proposed U-net extraction. This decrease in WBCs for U-net method on including edge thresholding is caused by decrease in contour areas of segmented WBCs after edge thresholding in some cases. Fig. 7 depicts this behavior and thus despite better segmentation due to edge thresholding as in Fig. 6 some components were not annotated as WBCs due to too smaller than 20% overlap of mask as in Fig. 7. Similar reasons apply to decrease in counts for few other types as well when edge thresholding was applied post U-net extraction.

We observed that the method by Liancheng *et al.* [11] extracted not only less artifacts but also less objects. For all the classes, as can be inferred from Table 2, the method by Liancheng *et al.* [11] underperformed even when compared with our proposed methods without edge thresholding. Fig. 8 shows some of the casts and Fig. 9 shows some of the yeasts that the method by Liancheng *et al.* [11] failed to extract while the proposed methods successfully extracted these objects. Also the method by Liancheng *et al.* [11] extracted some dark patch artifacts, which were caused by

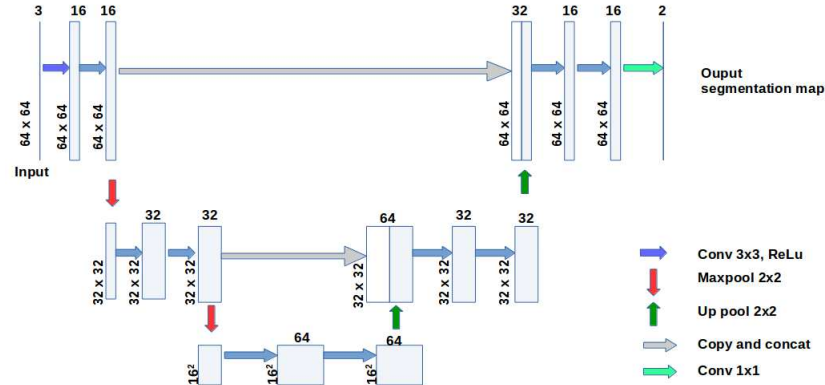


Figure 4. The U-net architecture corresponding to the best hyperparameters obtained via cross-validation on the validation set.

Class	Liancheng <i>et al.</i> [11]	Proposed unsupervised extraction	Proposed unsupervised extraction & edge thresholding	U-net	U-net & edge thresholding
Bacteria	16	<b>70</b>	<b>70</b>	<b>70</b>	<b>70</b>
Cast	5	38	38	<b>40</b>	<b>40</b>
Crystal	367	<b>667</b>	645	578	526
Epithelial	44	<b>72</b>	<b>72</b>	<b>72</b>	<b>72</b>
RBC	430	781	<b>1139</b>	775	913
WBC	733	663	<b>1165</b>	871	848
Yeast	13	<b>111</b>	79	93	78
Artifact	<b>2028</b>	2849	2262	2625	2663
Total objects	1608	2402	<b>3208</b>	2499	2547
Total Patches	3636	5251	<b>5470</b>	5124	5210
Artifact / Object ratio	1.26	1.19	<b>0.71</b>	1.05	1.05

Table 2. Image patch counts for different extraction techniques. Total patches include all the object types and artifacts. Artifact/Object ratio is the ratio of the count of extracted artifact patches to the count of total extracted object patches.

shadows of scratches in cover-slip glass. We did not observe these patches in any of the proposed methods. Some of these patches are shown in Fig. 10.

Now we discuss some cases where edge thresholding decreases the performance of a proposed method. As seen in Table 2, extraction methods that have edge thresholding failed to extract some of the crystals that were otherwise extracted by the corresponding methods without edge thresholding. The reason for this behavior is that some pixels were identified as edges and thus falsely removed by the edge thresholding method. Some example are shown in Fig. 11. Sometimes yeasts have small buds and edge thresholding may generate separated contours with very small area, which sometimes fail to pass the overlap criteria and are thus not extracted. Some examples of the yeast patches that were missed by edge thresholding techniques are shown in Fig. 12.

Another interesting finding is that the segmentation obtained using the method by Liancheng *et al.* [11] sometimes yields almost the entire FOV image as one single

component. On the other hand multiple components were extracted from the same FOVs using any of the proposed methods. One of such FOV is shown in Fig. 13 where the method by Liancheng *et al.* [11] extracted the entire FOV as a single component while the other technique extracted multiple components hence yielding more yeasts, casts and RBCs. One of the reason for this behavior is that the first thresholding technique in Liancheng *et al.* [11] is sensitive to contrast. In this case, this resulted in a noisy segmentation, which when post-processed yielded the entire FOV as a single component.

As discussed in Section 1, an important criterion of a good extraction method is to not only maximize the extraction of objects but to also minimize the extraction of artifacts. The lower the artifacts, the less error is propagated to the downstream processes such as classification and quantification. This led us to use object to artifact ratio as another criterion along with total objects extracted. As seen in Table 2, proposed unsupervised extraction with edge thresholding technique outperforms other methods with artifact to

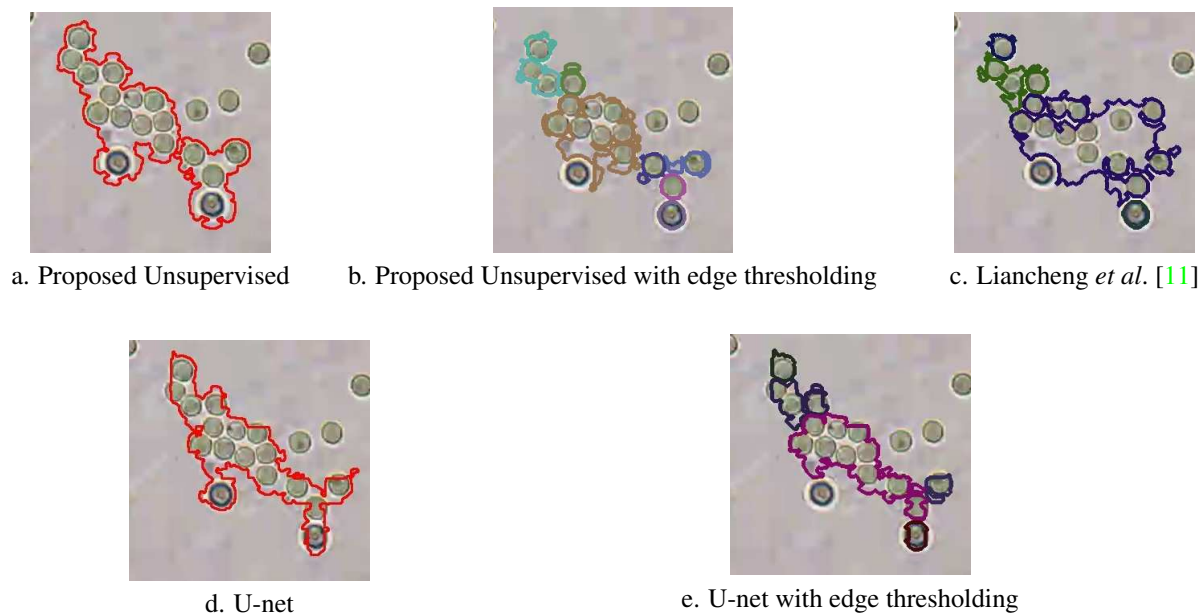


Figure 5. Segmentation mask boundaries for an RBC clump obtained using different methods. Different colors indicate different masks.

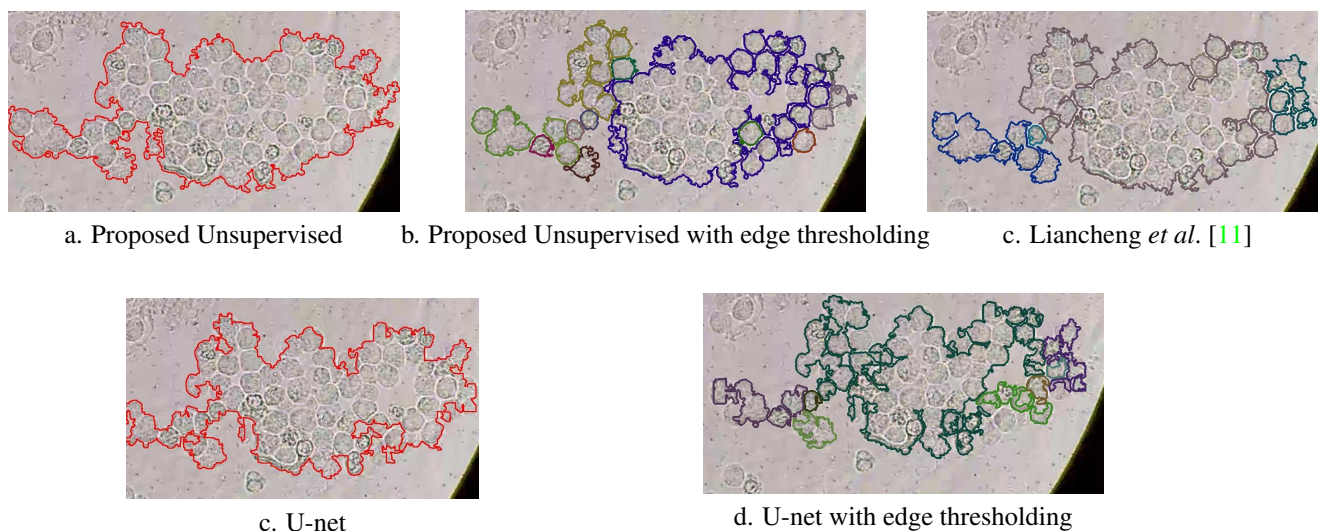


Figure 6. Segmentation mask boundaries for a WBC clump obtained using different methods. Different colors indicate different masks.

object ratio of 0.71, while this ratio for all the other methods is above 1. Also the proposed unsupervised method with edge thresholding extracted the maximum number of 3208 objects. Without edge thresholding, U-net outperformed the other methods on these two criteria. When different classes are individually examined in Table 2, different proposed methods performed better than the other methods. Recent Deep Learning methods are known to outperform conventional methods when large amounts of data is used for training. The higher performance of the proposed unsupervised method as compared to the Deep Learning-based U-net method is possibly due to lack of sufficiently large

data for training the Deep Learning method.

## 6. Conclusions

In this paper, we proposed both a novel unsupervised thresholding method and applied a supervised Deep Learning based U-net architecture for extracting objects from urine microscopic images. We also fused our proposed methods with an edge thresholding method from an existing work, which is helpful in segmenting adhesive cells. For different object types different proposed methods performed better than others, but over all the unsupervised method along with edge thresholding outperformed other

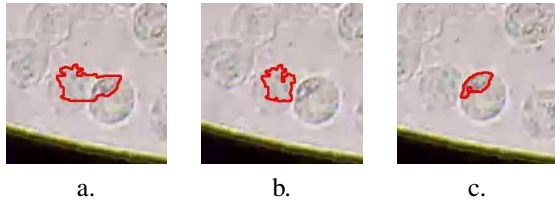


Figure 7. WBC masks comparison for U-net and U-net with edge thresholding. Figure (a) shows WBC mask with U-net only. Figure (b) and (c) shows the masks from U-net with edge thresholding. After edge thresholding, all though the cells segmented, the components didn't meet the 20% overlap criterion for selection.



Figure 8. Some of the casts that were missed by the method by Liancheng *et al.* [11] but extracted by both the proposed methods of unsupervised extraction, U-net based extraction and with and without edge thresholding. Mask boundaries in the above figures are from the unsupervised extraction method.

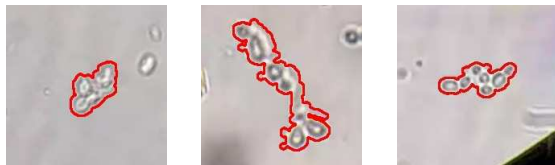


Figure 9. Some of the yeasts that were missed by the method by Liancheng *et al.* [11] but extracted by both the proposed methods of unsupervised extraction, U-net based extraction and with and without edge thresholding. Mask boundaries in the above figures are from the unsupervised extraction method.



Figure 10. Dark patches (artifacts) extracted by the method by Liancheng *et al.* [11] but these patches are not extracted by the proposed methods of unsupervised extraction, U-net based extraction and with and without edge thresholding.



Figure 11. Crystals that were extracted by the proposed methods without edge thresholding but missed by their counterpart methods with edge thresholding. Mask boundaries in the above figures are from the proposed unsupervised method. However these crystals were extracted by both the proposed methods of unsupervised extraction and U-net based extraction.

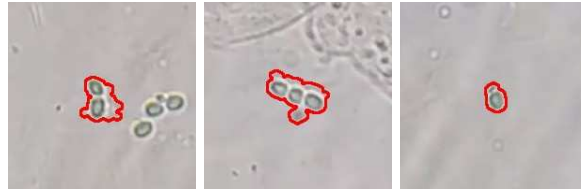
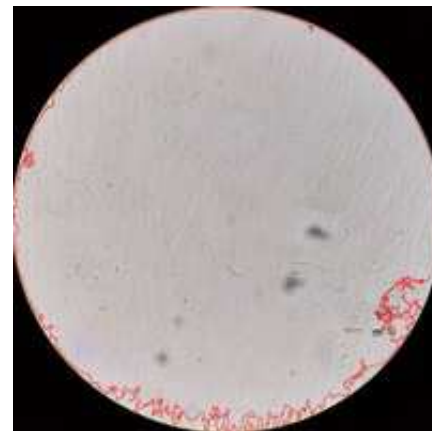
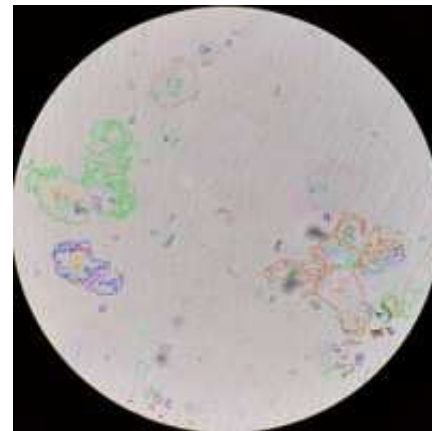


Figure 12. Yeast that were extracted by the proposed methods without edge thresholding but missed by their counterpart methods with edge thresholding. Mask boundaries in the above figures are from the proposed unsupervised method. However these yeast were extracted by both the proposed methods of unsupervised extraction and U-net based extraction.



a. Liancheng *et al.* [11]



b. U-net

Figure 13. Segmented mask boundaries using Liancheng *et al.* [11], which extracts a single huge component, while the proposed U-net method extracts multiple components. The other proposed methods produced similar segmentation as U-net. Different colors indicate different mask boundaries.

methods. Using experimental results, we demonstrate that the proposed extraction methods are very effective in urine object extraction and can be used as vital modules in an automated urine analyzer pipeline.

## References

- [1] G. Cao, C. Zhong, L. Li, and J. Dong. Detection of red blood cell in urine micrograph. In *International Conference on Bioinformatics and Biomedical Engineering*, pages 1–4. IEEE, 2009.
- [2] T. F. Chan and L. A. Vese. Active contours without edges. *IEEE Transactions on Image Processing*, 10(2):266–277, 2001.
- [3] Z. G. Chen, A. H. Chen, and Y. L. Cui. Segmentation of complex microscopic cell image based on contourlet and level set. In *Advanced Materials Research*, volume 429, pages 298–302. Trans Tech Publications, 2012.
- [4] S. Chourasiya and G. U. Rani. Automatic red blood cell counting using watershed segmentation. *International Journal of Computer Science and Information Technologies*, 5(4):4834–4838, 2014.
- [5] K. He, X. Zhang, S. Ren, and J. Sun. Deep residual learning for image recognition. In *Proceedings of the IEEE conference on computer vision and pattern recognition*, pages 770–778, 2016.
- [6] G. Huang, Z. Liu, K. Q. Weinberger, and L. van der Maaten. Densely connected convolutional networks. In *Proceedings of the IEEE conference on computer vision and pattern recognition*, volume 1, page 3, 2017.
- [7] X. Jiang and S. Nie. Urine sediment image segmentation based on level set and mumford-shah model. In *International Conference on Bioinformatics and Biomedical Engineering*, pages 1028–1030. IEEE, 2007.
- [8] A. Krizhevsky, I. Sutskever, and G. E. Hinton. Imagenet classification with deep convolutional neural networks. In *Advances in Neural Information Processing Systems*, pages 1097–1105, 2012.
- [9] C. Li, B. Fang, Y. Wang, G. Lu, J. Qian, and L. Chen. Automatic detecting and recognition of casts in urine sediment images. In *International Conference on Wavelet Analysis and Pattern Recognition*, pages 26–31. IEEE, 2009.
- [10] Y. Li and X. Zeng. A new strategy for urinary sediment segmentation based on wavelet, morphology and combination method. *Computer Methods and Programs in Biomedicine*, 84:162–173, 2006.
- [11] S. Liancheng, J. Shen, and W. Chenlu. A segmentation method based on standard difference gradient with dual-threshold for urinary sediment visible components. In *International Conference on Information Science and Control Engineering*, pages 94–98. IEEE, 2017.
- [12] J. Long, E. Shelhamer, and T. Darrell. Fully convolutional networks for semantic segmentation. In *Proceedings of the IEEE Conference on Computer Vision and Pattern Recognition*, pages 3431–3440, 2015.
- [13] H. Luo, S. Ma, D. Wu, and Z. Xu. Mumford-shah segmentation for microscopic image of the urinary sediment. In *International Conference on Bioinformatics and Biomedical Engineering*, pages 861–863. IEEE, 2007.
- [14] D. Mumford and J. Shah. Optimal approximations by piecewise smooth functions and associated variational problems. *Communications on Pure and Applied Mathematics*, 42(5):577–685, 1989.
- [15] W. Niblack. *An introduction to digital image processing*. Strandberg Publishing Company, 1985.
- [16] S. Osher and J. A. Sethian. Fronts propagating with curvature-dependent speed: algorithms based on hamilton-jacobi formulations. *Journal of Computational Physics*, 79(1):12–49, 1988.
- [17] N. Otsu. A threshold selection method from gray-level histograms. *IEEE transactions on Systems, Man, and Cybernetics*, 9(1):62–66, 1979.
- [18] S. M. Pizer, E. P. Amburn, J. D. Austin, R. Cromartie, A. Geselowitz, T. Greer, B. T. H. Romeny, J. B. Zimmerman, and K. Zuiderveld. Adaptive histogram equalization and its variations. *Computer Vision, Graphics, and Image Processing*, 39(3):355–368, 1987.
- [19] O. Ronneberger, P. Fischer, and T. Brox. U-net: convolutional networks for biomedical image segmentation. In *International Conference on Medical Image Computing and Computer-Assisted Intervention*, pages 234–241. Springer, 2015.
- [20] J. Sauvola and M. Pietikäinen. Adaptive document image binarization. *Pattern Recognition*, 33(2):225–236, 2000.
- [21] Z. Shi, Q. Jinlong, and Q. Guangjie. Urinary sediment overlapping cells image segmentation based on combination strategy. In *International Symposium on Computational Intelligence and Design*, volume 2, pages 3–7. IEEE, 2008.
- [22] K. Simonyan and A. Zisserman. Very deep convolutional networks for large-scale image recognition. *arXiv preprint arXiv:1409.1556*, 2014.
- [23] S. K. Strasinger and M. S. D. Lorenzo. *Urinalysis & Body Fluids 5TH EDITION*. F. A. Davis Company, 2008.
- [24] S. Suzuki and K. Abe. Topological structural analysis of digitized binary images by border following. *Computer Vision, Graphics, and Image Processing*, 30(1):32–46, 1985.
- [25] C. Szegedy, W. Liu, Y. Jia, P. Sermanet, S. Reed, D. Anguelov, D. Erhan, V. Vanhoucke, and A. Rabinovich. Going deeper with convolutions. In *Proceedings of the IEEE Conference on Computer Vision and Pattern Recognition*, pages 1–9, 2015.
- [26] Y. H. Wu and M. Kang. A urinary sediment segmentation algorithm of cast and epithelial cells. In *Frontiers of Mechanical Engineering and Materials Engineering II*, volume 457 of *Applied Mechanics and Materials*, pages 1046–1049. Trans Tech Publications, 2014.
- [27] S. Zhang, J. Wang, S. Zhao, and X. Luan. Urinary sediment images segmentation based on efficient gabor filters. In *International Conference on Complex Medical Engineering*, pages 812–815. IEEE, 2007.
- [28] Z. Zhang, S. Xia, and H. Duan. Cellular neural network based urinary image segmentation. In *International Conference on Natural Computation*, volume 2, pages 285–289. IEEE, 2007.
- [29] J. Zheng and Z. Chen. A fast urinary sediment image segmentation method. *Microcomputer Information*, 27(12):19–21, 2011.